Available online at www.sciencedirect.com
ScienceDirect
International Journal of Fatigue 30 (2008) 834–849
International Journal of Fatigue
www.elsevier.com/locate/ijfatigue

Fatigue of 7075-T651 aluminum alloy

Tianwen Zhao, Yanyao Jiang *

University of Nevada, Department of Mechanical Engineering, Mail Stop 312, Reno, NV 89557, USA

Received 29 November 2006; accepted 2 July 2007
Available online 2 August 2007

Abstract

Extensive fatigue experiments were conducted using 7075-T651 aluminum alloy under uniaxial, torsion, and axial-torsion loading. Detailed fatigue results were reported. Different mean stresses were applied in the experiments and the mean stress was found to have a significant influence on the fatigue strength of the material. A tensile mean stress decreased the fatigue strength dramatically. Fatigue damage was found to occur under compression–compression loading. In addition, axial-torsion experiments using tubular specimens were conducted under different loading paths to study the multiaxial fatigue behavior. Fatigue cracking behavior was found to be dependent on the loading path as well as the loading magnitude. When the loading magnitude was high, the material displayed shear cracking. When the loading stress was below a certain level, the material exhibited tensile cracking. For most loading cases under investigation, the material displayed a mixed cracking behavior. A kink was found in the shear strain versus fatigue life curve from the pure torsion experiments, and it was associated with a distinctive transition of cracking behavior. The Smith–Watson–Topper (SWT) parameter with a critical plane interpretation was found to correlate well with most of the experiments conducted in terms of fatigue lives. However, the SWT parameter cannot deal with the uniaxial fatigue conditions where the maximum stress is low or negative. More importantly, the model fails to correctly predict the cracking behavior observed experimentally on the material. A critical plane criterion based on a combination of the normal and shear components of the stresses and strains on material planes was found to better correlate the fatigue experiments in terms of both fatigue life and cracking behavior. The characteristics of the multiaxial fatigue criterion were discussed based on the experimental observations on 7075-T651 aluminum alloy.

Keywords: 7075-T651 aluminum alloy; Axial-torsion; Compression–compression fatigue; Multiaxial criterion; Multiaxial fatigue

1. Introduction

Aluminum alloys are widely used in the aircraft industry due to the high strength-to-density ratio. Extensive studies have been conducted to understand the fatigue behavior of aluminum alloys over the years. The fatigue process consists of crack initiation and crack propagation to failure. Smooth specimens are usually used to study the crack initiation behavior. Fatigue lives are related to the stress and strain quantities. Cracked specimens are used to investigate the crack growth behavior and often the fracture mechanics approaches are used to characterize crack propagation. Different approaches have been developed emphasizing either crack initiation or crack growth for the design and evaluation of a load-bearing structure. For example, there are two basic approaches currently used in the fatigue design in the US Navy and Air Force: "safe-life" and "damage tolerance" [1]. The first approach considers the fatigue crack nucleation only while the second approach predicts crack growth. The "safe-life" approach may be appropriate for the fatigue design of a structure while the "damage tolerance" approach may be more suitable for the evaluation of an existing component.

Although disputes exist with respect to a proper definition of crack initiation, it is an accepted conclusion that a majority of the life is spent on the crack initiation phase in the high cycle fatigue regime. New high strength alloys often have small critical flaw sizes and as a result, most of the lifetime of the structures made from these alloys is

* Corresponding author. Tel.: +1 775 784 4510; fax: +1 775 784 1701.
E-mail address: yjiang@unr.edu (Y. Jiang).

0142-1123/$ - see front matter © 2007 Elsevier Ltd. All rights reserved.
doi:10.1016/j.ijfatigue.2007.07.005

spent in initiating fatigue cracks. Knowledge and predictions of the crack initiation life are important for the assessment of the fatigue life of a structural component. Crack initiation behavior is the base for the crack growth predictions in a unified approach for fatigue life predictions [2].

Most experimental studies on aluminum alloys were concentrated on uniaxial tension–compression loading with the mean stress effects [3–6]. Stress–life and strain–life methods are often used based on the stabilized stress–strain hysteresis loops. It is often found that in the lower plastic strain region, the Coffin–Manson relationship does not obey the single slope behavior for the aluminum alloys. Endo and Morrow [3] observed that the usual linear log–log relationships between the fatigue life and the elastic and plastic strains did not provide an adequate correlation of the experimental results for 2024-T4 and 7075-T6 aluminum alloys. Sanders et al. [7] showed that the plots of the plastic strain amplitude versus the fatigue life for the aluminum alloys reflected the linearity of the Coffin–Manson relationship down to a critical level of plastic strain. The deviation of the fatigue results of the aluminum alloys from the single slope behavior of a Coffin–Manson plot was related to the relative inability of the microstructure to develop homogeneous slip during low plastic strain cycling. Fatemi et al. [8] applied a bi-linear relationship to the stress amplitude versus fatigue life curve of 14 aluminum alloys including 7075 aluminum alloy. It was shown that the bi-linear S–N model provided a better representation of the data than the commonly used single slope linear model.

Fracture mechanics approaches were also used to study the fatigue initiation life of aluminum alloys [9–11]. Short-crack analyses were used to simulate the total fatigue life (S–N) of unnotched specimens made of 7075-T6 and tested under constant amplitude loading [9]. Gill and Pao [10] detected fatigue crack initiation, determined the local notch tip stresses and strains, and compared the fatigue crack initiation of 7075 aluminum alloy in the as-polished condition and in the polished-and-pitted conditions. Döring et al. [11] developed a short crack model based on the integration of Paris type crack growth equation. The initial starter crack length is determined by using a backward integration of the Paris type law based upon the experimentally determined data from uniaxial loading. It was observed that cracked constituent particles constituted the majority of the observed fatigue crack nucleation sites in several aircraft aluminum alloys [12]. These constituent particles, which are inherent in the material, are formed during the cooling process when some of the alloying elements solidify more rapidly than the aluminum. The distribution of these particle sizes were treated as the initial crack sizes in predicting fatigue life [12]. A microstructure based multiscale fatigue model was developed to estimate the fatigue behavior for 7075 aluminum alloy with the consideration of damage incubation, microstructurally small crack growth, and long crack growth [13].

Engineering components often experience multiaxial stresses. A fatigue criterion is needed to assess the fatigue behavior under multiaxial stress loading. A major development in fatigue life predictions is the confirmation of the critical plane approaches for multiaxial fatigue. A critical plane approach concerns a critical plane in a given material for a known stress state on which cracks nucleate. The notion is that cracking behavior is material and loading magnitude dependent.

Smith, Watson, and Topper (SWT) [14] developed a fatigue model to consider the mean stress effect for uniaxial loading by using the cyclic strain amplitude and the maximum stress

$$\mathrm{FP} = \sigma_{\max}\frac{\Delta\varepsilon}{2} \tag{1}$$

where $\Delta\varepsilon/2$ is the strain amplitude and $\sigma_{\max}$ is the maximum stress in a loading cycle. FP denotes "fatigue parameter". Socie [15] extended the SWT parameter to multiaxial fatigue with a critical plane interpretation. The critical plane was defined as the material plane where the normal strain amplitude was a maximum. The normal strain amplitude, $\Delta\varepsilon/2$, and the maximum normal stress, $\sigma_{\max}$, in Eq. (1) are taken on the critical plane. For tension–compression loading, the criterion predicts a cracking plane with its normal being parallel to the axial stress direction. The criterion predicts $\pm 45°$ cracking planes under pure torsion loading. It has been commonly recognized that the SWT parameter is particularly suitable for aluminum alloys.

Despite comprehensive work, many questions remain to be answered. Limited efforts have been made on the multiaxial fatigue study of the aluminum alloys. Particularly, the cracking behavior of the aluminum alloys under different stress states has not been well investigated. In the current study, extensive fatigue experiments were conducted using 7075-T651 aluminum alloy under uniaxial, torsion, and axial-torsion loading. Different mean stresses were applied in the experiments to study the mean stress effects on fatigue. Cracking behavior under different stress states was studied. Fatigue under compression–compression loading was experimentally investigated. The SWT fatigue criterion with the critical plane interpretation and a modified SWT parameter were evaluated based on the experimental results.

2. Experiments

2.1. Material and specimens

The material used in the current experimental investigation was 7075-T651aluminum alloy. As shown in Fig. 1, four types of testing specimens were used in the testing program. They were uniaxial dog-bone shaped plate specimens (Fig. 1a), uniaxial solid cylindrical specimens (Fig. 1b), solid cylindrical specimen for torsion (Fig. 1c), and tubular specimens for axial-torsion loading (Fig. 1d). The dog-bone plate specimens were machined from a large plate.

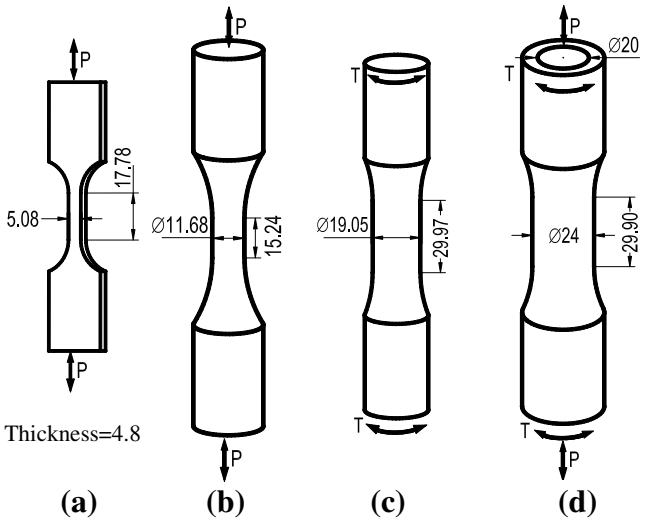

Fig. 1. Specimens and loading conditions (all dimensions in mm).

Both the uniaxial cylindrical solid specimen and the specimens for torsion were fabricated from a cylindrical bar with a diameter of 25.4 mm. A solid bar with a diameter of 38 mm was used to fabricate the tubular specimens.

Since the cold-rolled materials were acquired commercially in different stocks, an inspection of the microstructure may help identify whether or not the materials were practically identical. Fig. 2 shows the optical microstructures of the three batches of the materials used in the current investigation. Each stereography was synthesized from three microstructures taken on the sections perpendicular to the rolling (x)-direction, the normal (y)-direction, and the transversal (z)-direction. The etchant used in microscopic examination was Keller's reagent (2 ml HF (48%), 3 ml HCl, 5 ml HNO_3, 190 ml H_2O). Dark particle-like precipitates in the microstructures are $Cr_2Mg_3Al_{18}$ and $(Fe,Mn)Al_6$.

For the plate specimen, equiaxial grains were observed on the rolling plane (section perpendicular to the normal direction). The grain size varies from 10 μm to 100 μm. The average grain size is approximately 50 μm. On the sections perpendicular to the rolling direction and the transverse direction, fibrous grains were observed. The average thickness of grains is approximately 7 μm. It is a typical microstructure after cold rolling (disk-like grains).

For the cylindrical specimens (Fig. 1b and c) made from a 25.4 mm diameter bar, the grains appear equiaxial on the section perpendicular to the axis. The grain size ranges from 10 μm to 40 μm. On the section parallel to the axis, fibrous grains are observed. The average length of grains along axial direction is about 70 microns. It is a typical microstructure after cold-drawn or cold extrusion (fibrous grains). Tubular specimens were machined from rod-shaped rod with a diameter of 38 mm. The microstructures are practically identical to these of the 25.4 mm diameter bar.

2.2. Experiments and results

An Instron Servohydraulic tension–torsion load frame was used for the fatigue experiments using the solid cylindrical specimens and the tubular specimens shown in Fig. 1. The testing system, which has a capacity of ±2800 N m in torque and ±222 kN in axial load, is equipped with the Instron 8800 electronic control, computer control, and data acquisition. A 12.7 mm gage length uniaxial extensometer was used for the measurement of the strain in the gage section of the uniaxial specimen. The extensometer has a range of ±5% strain. For the tubular specimens and the specimens for torsion, a modified MTS extensometer was attached to the gage section of the specimen to measure the axial, shear, and diametral strains. The extensometer had a range of ±5% in the axial strain, a range of ±3° in the torsion deformation, and 0.25 mm in the diametral direction. An Instron 8870 load frame with 8800 electronics and computer control was used for some of the uniaxial fatigue experiments using the plate specimens. The load cell of the testing machine has a capability of ±25 kN axial load. All the experiments were conducted in ambient air.

Regular monotonic experiments were conducted to determine the static material properties of the material and the results are summarized in Table 1. The true fracture stress and the true fracture strain of the material were obtained by conducting a monotonic torsion experiment using the solid shaft specimen (Fig. 1c). Fig. 3 shows the shear stress–shear strain curve obtained from a round solid specimen subjected to monotonic torsion. The surface

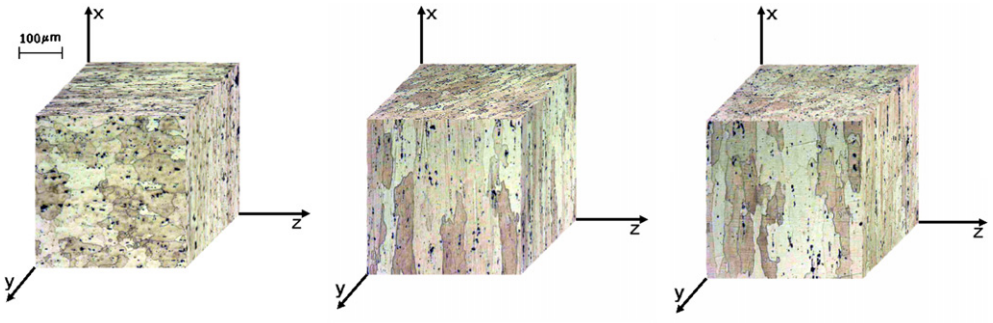

Fig. 2. Stereographic microstructure of the material.

Table 1
Static material properties of 7075-T651

Elasticity modulus, E	71.7 GPa
Shear modulus, G	27.5 GPa
Poisson's ratio, μ	0.306
Yield stress, $\sigma_{0.2}$	501 MPa
Ultimate strength, S_u	561 MPa
Elongation, e_f	9.7%
Reduction in area, RA	29.1%
True shear fracture stress, τ_f	379 MPa
True shear fracture strain, γ_f	0.384

strain was measured by using an extensometer and the surface stress was determined following the Nadai's formula [16]. The torsion of a solid shaft can provide an experimental means to determine the true fracture stress and true fracture strain.

Fig. 4 shows the six loading paths used in the axial-torsion experiments for the tubular specimens. Fig. 4a is pure shear loading, and Fig. 4b is the loading case with fully reversed shear and a static axial stress. Fig. 4c is the proportional loading path. Fig. 4d is a circular shaped axial-torsion nonproportional loading path. Loading paths shown in Figs. 4e and f are nonproportional loading paths with the ratios of the torsion loading frequency over the axial loading frequency being two and four, respectively.

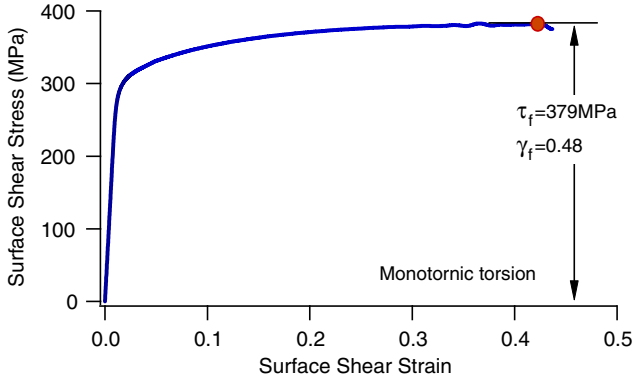

Fig. 3. Shear stress–shear strain curve obtained from monotonic torsion of solid shaft specimen.

Considering the value of the experimental fatigue data, it was considered desirable to tabulate all the detailed fatigue results obtained from the current investigation. Uniaxial specimens (Fig. 1a and b) were tested to complete failure. For tubular specimens (Fig. 1d), the reported fatigue life corresponded to the moment when the stress amplitude was reduced by 10% from the stabilized value or a visible crack was found on the surface of the testing specimen. For any specimen when the testing was terminated, a visible crack can be found on the specimen surface. Stress and strain measurements listed in the tables were taken from representative cycles at approximately 50% of the failure life. Detailed experimental fatigue results are listed in Tables 2–5.

Figs. 5 and 6 show the basic fatigue data and fatigue cracking behavior obtained from the fully reversed uniaxial loading. A data point followed by a horizontal arrow denotes a run-out fatigue experiment. It is evident that the plate specimens with two different orientations and the solid dog-bone cylindrical specimens yielded very similar fatigue results. The detailed stress amplitude, strain amplitude, and fatigue life for each fully reversed uniaxial experiment are listed in Table 2.

The following three-parameter equation is used to describe the strain–life curve for the fully reversed unixial fatigue by best fitting the experimentally obtained data,

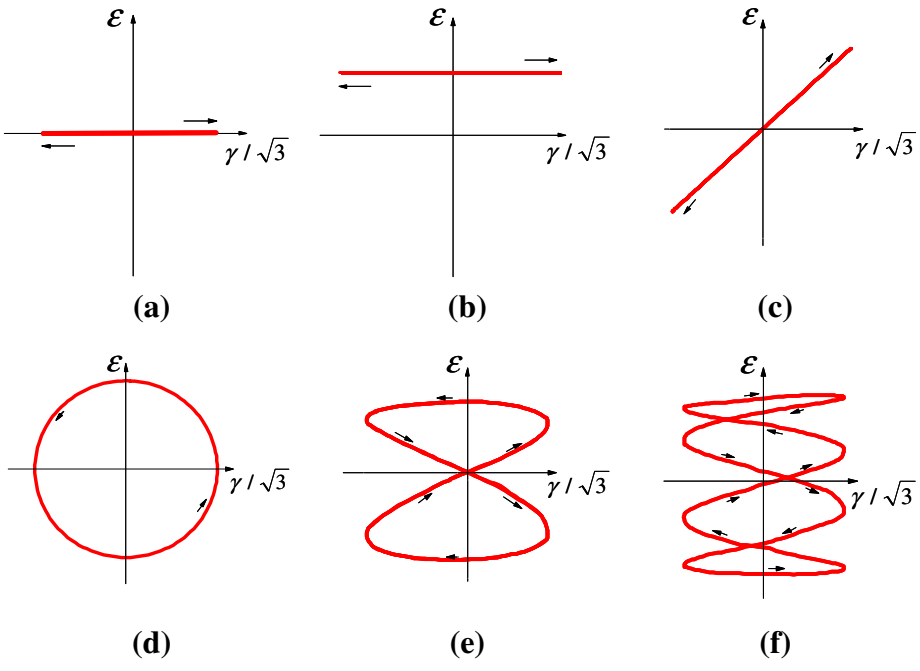

Fig. 4. Loading paths for axial-torsion loading using tubular specimens.

Table 2
Results from plate and dog-bone cylindrical uniaxial specimens

Spec No.	$\frac{\Delta\varepsilon}{2}$(%)	$\frac{\Delta\sigma}{2}$(MPa)	σ_m(MPa)	f(Hz)	N_f(cycles)	Spec No.	$\frac{\Delta\varepsilon}{2}$(%)	$\frac{\Delta\sigma}{2}$(MPa)	σ_m(MPa)	f(Hz)	N_f (cycles)
a) Dog-bone cylindrical uniaxial specimens under fully reversed strain-controlled loading											
TorS43	3.09	630.8	−0.2	0.125	25	TorS37	0.51	361.6	−3.6	1	9,112
TorS45_2	2.55	614.0	−2.3	0.125	58	TorS32	0.42	299.6	1.5	1	27,011
TorS41	2.02	592.9	−3.3	0.125	73	TorS33	0.34	240.0	1.1	2	99,287
TorS44	1.53	567.5	−5.2	0.25	125	TorS38	0.28	200.2	0.6	6	919,687
TorS39_2	1.23	555.2	−7.8	0.25	194	TorS34_1	0.21	150.0	0.4	10	>1,063,477
TorS40	1.02	533.8	−7.2	0.25	390	TorS45_1	0.30	214.9	1.0	10	>1,090,639
TorS34_2	0.81	512.2	−7.3	0.25	794	TorS39_1	0.29	210.1	1.4	10	>1,108,763
TorS36	0.72	485.5	8.9	0.5	917						
TorS35	0.56	400.1	2.8	0.5	3,073						
TorS42	0.49	349.7	2.1	1	7,144						
b) 0° plate specimen											
0-56	4.00	627.5	3.5	0.075	5	0-17	0.29	210.2	15.5	10	109,557
0-55	3.92	625.2	5.7	0.1	7	0-12	0.27	191.4	0.7	10	116,333
0-53	2.92	600.1	−1.3	0.1	14	0-41	0.22	157.0	0.7	5	182,900
0-52	2.43	584.5	−2.9	0.125	15	0-28	0.24	167.4	0.6	10	624,994
0-51	2.44	583.8	−1.8	0.25	34	0-29	0.21	154.1	−0.1	10	1,079,668
0-34	1.53	537.9	−4.3	0.25	45	0-25	0.40	268.1	268.2	2	5,275
0-39	1.23	528.4	−8.7	0.25	112	0-19	0.41	284.7	221.3	2	6,144
0-32	1.02	511.5	−9.3	0.25	200	0-23	0.40	280.1	159.9	2	12,288
0-57	0.91	509.5	−13.2	0.5	415	0-22	0.32	220.1	220.0	2	17,885
0-33	0.82	493.2	−7.4	0.5	512	0-21	0.29	200.5	200.5	5	34,956
0-10	0.71	489.3	0.2	0.5	945	0-24	0.25	177.6	177.7	5	54,680
0-18	0.65	488.4	−39.0	0.5	713	0-20	0.21	146.6	146.6	10	209,237
0-03	0.60	434.5	−36.0	1	3,357	0-27	0.19	133.0	133.1	10	1,075,867
0-16	0.61	435.7	73.0	1	2,055	0-26	0.17	118.7	118.7	10	>1,283,726
0-36	0.64	455.5	−5.8	1	2,635	0-67	0.19	143.9	240.4	10	79,324
0-05	0.46	333.2	−22.2	2	9,010	0-69	0.67	455.5	54.2	1	871
0-01	0.51	368.8	−54.4	1	11,504	0-68	0.58	404.0	103.8	1	1,045
0-15	0.41	301.8	39.1	5	22,121	0-70	0.50	353.7	152.5	2	2,862
0-38	0.42	299.3	1.3	4	27,788	0-71	0.29	203.2	303.5	5	7,315
0-04	0.42	299.3	−34.4	5	40,930	0-73	0.22	153.0	354.8	10	14,782
0-31	0.37	262.4	1.2	5	47,740	0-72	0.17	121.7	384.6	10	24,979
0-06	0.36	258.1	1.2	10	55,470	0-54	0.16	108.4	497.5	5	11,639
0-07	0.31	222.1	1.0	10	51,717	0-59	0.11	75.7	432.1	10	245,801
0-35	0.31	222.0	1.1	5	58,666	0-55	0.10	70.7	435.8	10	>1,608,028
c) 90° plate specimen											
90-69	3.51	633.7	−5.3	0.125	4	90-31	0.23	161.9	0.5	10	>1,450,963
90-41	0.97	515.9	−15.2	0.5	175	90-30	0.22	155.3	0.4	10	>1,117,723
90-37	1.07	522.1	−14.3	0.25	232	90-24	0.40	268.1	268.0	2	4,012
90-39	0.72	478.8	−14.6	1	759	90-19	0.42	293.1	92.4	2	20,691
90-09	0.77	497.2	−21.7	0.5	788	90-21	0.32	222.2	221.9	2	20,306
90-13	0.70	486.0	−7.4	0.5	884	90-22	0.29	200.5	200.4	5	25,645
90-17	0.73	492.7	11.5	0.5	1,212	90-23	0.25	175.9	175.9	5	45,294
90-40	0.62	439.9	3.2	2	1,265	90-25	0.25	175.7	175.8	5	45,967
90-06	0.62	444.0	−9.9	2	1,880	90-26	0.19	133.0	133.0	10	196,177
90-15	0.67	473.7	−17.6	1	2,268	90-28	0.18	127.2	127.3	10	210,014
90-18	0.47	395.9	−44.7	1	2,299	90-20	0.21	147.7	147.6	10	227,619
90-02	0.53	378.3	−31.3	2	4,429	90-34	0.18	122.8	122.8	10	716,425
90-42	0.52	370.2	2.7	4	9,035	90-29	0.18	124.8	124.8	10	932,194
90-07	0.42	300.1	−19.6	5	18,120	90-27	0.17	120.1	120.1	10	>1,271,590
90-14	0.48	349.3	−16.9	5	21,053	90-35	0.17	121.2	121.3	10	1,415,524
90-08	0.36	259.9	1.3	10	40,443	90-58	1.12	557.7	69.0	0.25	17
90-03	0.35	250.0	1.2	10	42,650	90-59	0.96	549.2	95.5	0.25	22
90-10	0.32	222.6	1.0	10	104,240	90-60	0.72	507.3	129.4	0.25	405
90-16	0.32	228.3	−12.5	10	164,041	90-61	0.46	323.5	282.9	2	1,674
90-12	0.28	190.6	0.7	10	131,072	90-62	0.31	218.1	390.0	5	3,649
90-38	0.22	161.6	0.1	5	394,116	90-53	0.15	101.8	405.8	10	28,813
90-32	0.24	173.7	0.4	10	625,893	90-52	0.12	82.0	425.5	10	141,596
90-66	0.21	144.8	−0.8	10	865,205	90-55	0.13	91.9	413.7	10	233,252
90-33	0.23	168.4	0.6	10	1,091,584						

$\Delta\varepsilon/2$ = axial strain amplitude, $\Delta\sigma/2$ = axial stress amplitude, σ_m = mean stress, N_f = fatigue life.
Note: TorSxx_1 (xx is the specimen number) was tested without failure and TorSxx_2 was the same specimen tested after the first step. The second step usually had a much higher load amplitude than that of the first step.

Table 3
Uniaxial loading with compressive mean stress

Spec No.	$\frac{\Delta\varepsilon}{2}$(%)	$\frac{\Delta\sigma}{2}$ (MPa)	σ_m(MPa)	f(Hz)	N_f (cycles)	Spec No.	$\frac{\Delta\varepsilon}{2}$(%)	$\frac{\Delta\sigma}{2}$ (MPa)	σ_m(MPa)	f(Hz)	N_f (cycles)
a) One step loading											
0-74	0.55	397.0	−96.9	2	6,513	0-66	0.35	313.1	−278.8	10	464,808
0-76	0.48	347.4	−147.0	5	18,217	90-51	0.27	198.7	−99.9	10	368,183
0-75	0.41	297.1	−197.0	5	115,601	90-56	0.40	295.5	−246.4	10	405,747
0-58	0.40	310.2	−262.6	10	212,001	90-63	0.38	316.3	−285.6	10	429,914
0-77	0.34	249.2	−148.2	10	222,563	90-64	0.40	315.0	−292.1	10	565,104
0-60	0.38	278.6	−215.0	10	226,682	90-57	0.37	273.3	−223.5	10	603,299
0-61	0.32	237.5	−161.6	10	288,283	90-65	0.38	315.3	−297.6	10	696,820
0-64	0.31	228.3	−169.1	10	291,220	90-72	0.39	300.9	−302.1	10	750,172
0-65	0.41	305.0	−268.1	10	383,667	90-68	0.39	307.0	−298.2	10	1,098,940
0-63	0.37	274.0	−221.5	10	406,747						

Spec No.	Step	$\frac{\Delta\varepsilon}{2}$(%)	$\frac{\Delta\sigma}{2}$(MPa)	σ_m(MPa)	f(Hz)	N(cycles)
b) Plate and cylindrical specimens under compression-compression, two step loading						
90-67	I	0.41	305.3	−291.1	10	498,374
	II		100.0	100.0	10	62
90-71	I	0.42	301.4	−292.6	10	472,623
	II		100.0	100.0	10	52
90-73	I	0.38	300.8	−310.3	10	802,796
	II		100.0	100.0	1	419
90-74	I	0.38	292.2	−311.8	10	880,885
	II		100.0	100.0	10	1,926
90-75	I	0.44	289.3	−300.3	10	397,716
	II		100.0	100.0	10	15,473
90-77	I	0.40	298.3	−299.2	10	375,132
	II		100.0	100.0	10	3,198
90-78	I	0.36	274.4	−322.1	10	982,635
	II		100.0	100.0	1	19,335
TorS21	I	0.41	308.1	−318.4	10	1,000,000
	II		100.0	100.0	10	29,831
TorS22	I	0.42	307.4	−317.2	10	2,000,000
	II		100.0	100.0	10	23,867
TorS23	I	0.39	285.8	−290.4	10	1,371,663
	II		100.0	100.0	10	15,353
TorS24	I	0.39	288.9	−283.5	10	2,781,162
	II		100.0	100.0	10	49,221

$\Delta\varepsilon/2$ = axial strain amplitude, $\Delta\sigma/2$ = axial stress amplitude, σ_m = mean stress, N_f = fatigue life.

$$\left(\frac{\Delta\varepsilon}{2}-\varepsilon_0\right)^{\xi} N_{\mathrm{f}} = C \tag{2}$$

where $\Delta\varepsilon/2$ is the strain amplitude and N_{f} is the number of cycles to failure. The remaining three symbols, ε_0, ξ and C, are constants obtained by best fitting the experimental data. For 7075-T651, $\varepsilon_0 = 0.0015$, $\xi = 3$, and $C = 0.0003$. The dot lines in Fig. 5 are the factor-of-five boundaries from that described by Eq. (2). These two lines also show the approximate scatter of the experimental fatigue life data of the material under investigation.

A careful examination of the cracking behavior of the fully reversed uniaxial loading specimens reveals that when the fatigue lives are longer than 2000 cycles, the cracking planes are consistently perpendicular to the loading axis. When the fatigue lives are lower than 100 cycles, the normal of the cracking planes approaches ±45° from the loading axis. When the fatigue lives are in between 100 and 2000 cycles, the normal of the cracking plane from the loading axis varies from zero to ±45°. A shear crack can grow in one of two ways [15], illustrated by Case A and Case B in Fig. 5. Case A crack is due to the in-plane shear stress. Case B cracks are the result of out-of-plane shear. Case A and Case B cracking were observed when the fatigue lives are less than 2000 cycles. Over the range of the fatigue lives investigated, a smooth transition of the cracking behavior and a statistically smooth strain–life curve were observed from the specimens under fully reversed uniaxial loading.

Uniaxial fatigue experiments were conducted with R-ratios ranging from $-\infty$ to 0.72, where R is the ratio of the minimum stress over the maximum stress in a loading cycle. The fatigue results are shown in Figs. 7 and 8, where Fig. 7 is the strain–life curve and Fig. 8 is the stress–life plot. The solid line in Fig. 7 is the strain–life curve described by Eq. (2) by best fitting the fully reversed uniaxial fatigue data. The detailed fatigue results under uniaxial loading are listed in Tables 2 and 3. Figs. 7 and 8 clearly show that the mean stress has a significant influence on fatigue life.

A number of uniaxial specimens were tested under the compression–compression condition with a zero or negative maximum stress in a loading cycle. In order to assess fatigue

Table 4
Pure torsion and cyclic torsion with static axial load for tubular specimens

Load Path	SpecNo.	σ_m(MPa)	$\frac{\Delta\gamma}{2}$(%)	$\frac{\Delta\tau}{2}$ (MPa)	f(Hz)	N_f(cycles)	Observed Cracking Direction θ^o
(a)	Tu31_2	0	1.97	335.2	0.25	152	90
	Tu18	0	1.73	340.0	0.25	209	90
	Tu17	0	1.21	315.7	0.5	670	5
	Tu42_2	0	1.07	286.6	0.5	1807	90
	Tu35	0	0.93	251.0	2	3,537	90
	Tu16	0	0.93	254.2	1	4,291	90
	Tu36	0	0.75	203.3	7	18,842	90
	Tu30	0	0.80	219.0	1	20,271	90
	Tu15	0	0.69	190.3	2	178,065	2
	Tu27	0	0.60	167.8	5	308,144	−42
	Tu24	0	0.69	192.0	2	328,816	−3
	Tu10	0	0.50	136.5	2	403,731	45
	Tu34	0	0.55	146.9	6	428,510	−43
	Tu28	0	0.40	110.8	5	805,783	46
	Tu37	0	0.46	124.5	2	913,545	−48
	Tu31_1	0	0.45	125.8	5	>1,005,181	–
	Tu39	0	0.36	101.0	7	3,867,638	45
(b)	Tu22	200.0	0.69	188.5	2	12,739	0
	Tu23	−200.0	0.69	192.0	2	52,986	90
	Tu25	293.1	0.69	189.8	1	4,394	0
	Tu26	−293.1	0.69	196.7	2	84,946	90
	Tu40	289.8	0.50	134.2	1	30,192	0
	Tu41	288.7	0.50	135.4	2	25,167	0
	Tu42_1	−296.4	0.51	138.8	4	>2,609,732	–
	Tu44_1	−389.1	0.50	135.6	4	>2,216,739	–
	Tu44_2	391.6	0.50	131.6	0.5	14,489	0

σ_m = static axial stress, $\Delta\gamma/2$ = shear strain amplitude, $\Delta\tau/2$ = shear stress amplitude, N_f = fatigue life.
Note: Tu31_1 was tested without failure and the specimen was tested at a much higher amplitude in a second step Tu31_2.

Table 5
Fatigue experiments conducted using tubular specimens

Load path	Spec No.	$\frac{\Delta\varepsilon}{2}$ (%)	$\frac{\Delta\gamma}{2}$ (%)	$\frac{\Delta\sigma}{2}$(MPa)	$\frac{\Delta\tau}{2}$(MPa)	f(Hz)	N_f(cycles)	Observed Cracking Direction θ^o
(c)	Tu06_2	0.64	1.1	370.0	222.9	0.2	147	90
	Tu04	0.50	0.86	351.3	222.0	0.25	1,967	23
	Tu19	0.22	0.78	165.6	216.2	1	9,174	90
	Tu20	0.17	0.6	127.2	170.5	2	59,194	87
	Tu33	0.23	0.4	166.1	110.4	5	136,646	−30
	Tu05	0.28	0.49	201.3	130.0	0.5	45,500	−32
	Tu32	0.21	0.37	153.5	100.3	2	662,627	−23
	Tu06_1	0.19	0.29	137.4	79.7	2	>1,018,000	–
	Tu29_1	0.18	0.36	132.4	96.8	4	>1,031,190	–
(d)	Tu29_2	0.85	1.45	543.7	329.4	0.25	146	5
	Tu02_2	0.75	1.30	497.7	319.1	0.25	424	−3
	Tu01	0.51	0.87	377.6	241.8	0.5	2,487	−2
	Tu21	0.38	0.66	280.4	181.8	1	10,191	0
	Tu11	0.28	0.49	200.9	131.6	1	29,439	−27
	Tu03	0.27	0.41	200.6	115.8	1	41,747	7
	Tu02_1	0.19	0.27	143.1	76.4	2	>632,258	–
(e)	Tu09	0.49	0.86	352.0	232.0	0.25 / 0.5	755	7
	Tu07	0.28	0.49	205.8	137.5	0.5 / 1	35,804	16
	Tu08	0.20	0.32	147.5	86.9	1 / 2	225,000	−22
(f)	Tu13	0.36	0.63	258.2	175.6	0.25 / 1	1,145	−34
	Tu14	0.40	0.70	295.0	197.2	0.25 / 1	2,301	−4
	Tu12	0.28	0.49	203.8	136.3	0.5 / 2	12,708	23

$\Delta\varepsilon/2$ = axial strain amplitude, $\Delta\gamma/2$ = shear strain amplitude, $\Delta\sigma/2$ = axial stress amplitude, $\Delta\tau/2$ = shear stress amplitude, N_f = fatigue life.
Note: Tuxx_1(xx is the specimen number) was tested without failure and Tuxx_2 was the same specimen continuously tested at a much higher loading amplitude. For loading path (e) and (f), the frequencies for tension and torsion are different. The number before the slash denotes the frequency for tension loads and the number after the slash denotes the frequency for torsion loads.

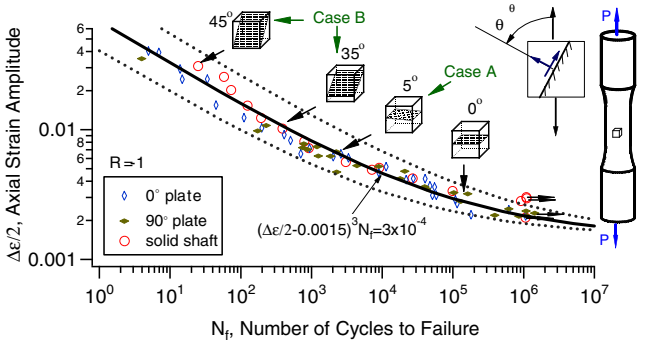

Fig. 5. Strain–life and cracking behavior under fully reversed uniaxial loading.

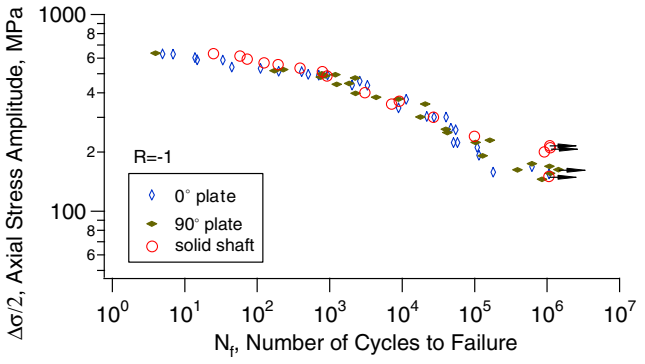

Fig. 6. Stress–life under fully reversed uniaxial loading.

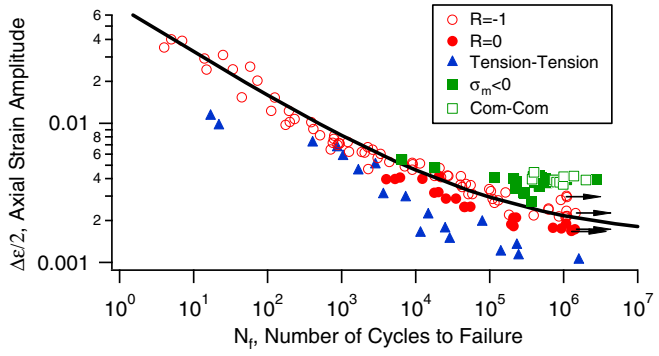

Fig. 7. Strain–life of all the uniaxial fatigue experiments conducted.

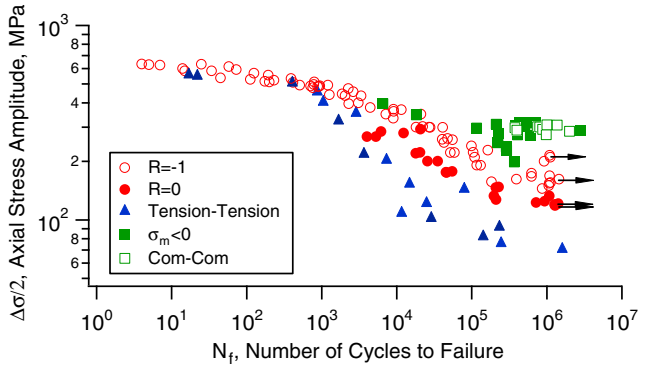

Fig. 8. Stress–life of all the uniaxial fatigue experiments conducted.

damage under compression–compression loading, a specimen was subjected to a designated compression–compression loading for up to 10^6 loading cycles. This was followed by a stress-controlled loading with $R = 0$ and a stress amplitude of 100 MPa. According to the results shown in Fig. 8, a stress amplitude of 100 MPa with $R = 0$ would result in a fatigue life longer than 10^7 loading cycles. Since fatigue cracks were often initiated on the material plane with its normal along the loading axis (the crack plane was perpendicular to the loading direction), failure of the specimen was difficult to identify under compression–compression loading. The two-step loading can help identify whether or not the compression–compression generated fatigue damage. If the number of loading cycles in the second loading step is significantly long, this may indicate that the fatigue damage created under the first step compression–compression may not have contributed to the fatigue damage. If the specimen fails in the second loading step within a number of loading cycles that is much less than 10^7, the first loading step must have generated significant fatigue damage.

Table 3b lists 11 specimens that were subjected to two-step loading. Among the 11 specimens, eight specimens were tested under the compression–compression loading conditions in the first loading step and failed in the second step loading. The numbers of loading cycles in the second loading steps were very limited. The results suggest that fatigue damage was developed under compression–compression loading. In fact, the results show that fatigue damage has reached a failing point already before the application of the second loading step.

Fig. 9 shows the fatigue results obtained from the pure shear experiments and the fatigue experiments conducted with cyclic shear combined with a static axial stress (loading path (b) in Fig. 4). Detailed data is listed in Table 4. Typical cracking behavior is also shown in the figure. The solid circles in Fig. 9 denote the results of pure torsion and the open markers are those under fully reversed torsion with static axial load. Two shear strain amplitudes, 0.50% and 0.69%, were used for loading path (b) shown in Fig. 4. The results shown in Fig. 9 reveal that a positive static axial static stress significantly reduced the fatigue life. When a compressive axial load was applied when the shear strain amplitude was 0.69%, the influence of the compres-

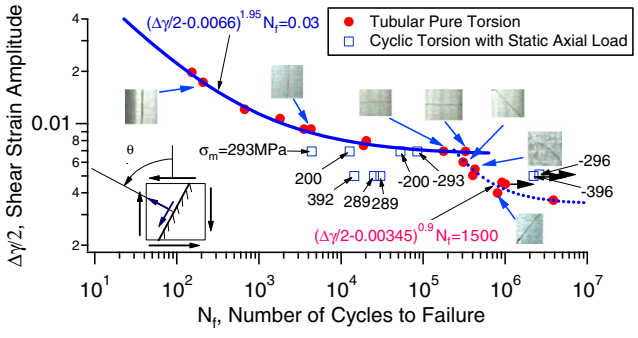

Fig. 9. Shear strain amplitude versus fatigue life for pure torsion and torsion with a static axial stress.

sive axial load was not detectable with the limited number of specimens tested. The compressive axial load clearly enhanced the fatigue life in the cases with the shear strain amplitude being 0.50%. A crack along the axial direction (the normal of the plane is perpendicular to the axial direction) was observed for the specimen tested under fully reversed shear with a compressive static axial stress. The cracking plane is perpendicular to the axial direction when the static axial stress is positive. The observations are consistent with that made by Socie and co-workers for Inconel 718 [21] under a similar loading condition.

A kink around a fatigue life of 3×10^5 cycles was noticed in the shear strain–life curve from pure torsion (Fig. 9). Unlike the strain–life for the uniaxial loading (Fig. 5) which can be properly described by using the three-parameter equation Eq. (2), the shear strain–life curve can be better described by two curves of the three-parameter equation mathematically identical to Eq. (2) as shown in Fig. 9. A further observation of the tested pure shear specimens revealed that the kink in the strain–life curve was associated with the cracking behavior. When the fatigue lives were less than 3×10^5 cycles, the cracking planes were either perpendicular or parallel to the specimen axis. In other words, cracks were found on the maximum shear planes. When the fatigue lives were higher than 3×10^5 cycles, cracks were consistently found to form on the maximum tensile planes (±45° from the specimen axis).

Changes of cracking behavior with the loading magnitude or fatigue life were observed on AISI 304 stainless steel [15], Inconel 718 [21], 1045 steel [22], and an aluminum alloy [23]. However, no kink in the strain–life curves was found to associate with the cracking behavior transition in these materials. Different slopes or discontinuous stress–life curves were often reported from the uniaxial tension–compression experiments for ultra high fatigue lives [17,18]. It is a common observation that kink in the stress–life curve is associated with the crack initiation sites in the specimen. When the fatigue lives are lower, fatigue cracks are initiated on the specimen surface. Crack initiation is often found to occur on subsurface from sites of interior defects.

Fig. 10 summarizes the results obtained from testing the tubular specimens under combined axial-torsion loading. Detailed experimental results are listed in Table 5. An equivalent strain amplitude is used to represent the loading magnitude under cyclic loading. The equivalent strain amplitude is defined as follows:

$$\left(\frac{\Delta\varepsilon}{2}\right)_{eq} = \sqrt{\left(\frac{\Delta\varepsilon}{2}\right)^2 + \frac{1}{3}\left(\frac{\Delta\gamma}{2}\right)^2} \tag{3}$$

where $(\Delta\varepsilon/2)_{eq}$ is the equivalent strain amplitude, $\Delta\varepsilon/2$ is the axial strain amplitude, and $\Delta\gamma/2$ is the shear stress amplitude. The fatigue experimental results obtained from testing the tubular specimens will be used to evaluate the fatigue models. It should be noted that the only purpose to use of the equivalent strain is to present the results with a simple and single plot.

3. Smith, Watson, and Topper (SWT) criterion

The Smith, Watson, and Topper (SWT) [14] criterion has been known to correlate well with the fatigue experiments of aluminum alloys. The critical plane extension of the SWT criterion is considered in the current investigation. Fig. 11 shows the SWT parameter versus the fatigue life for the uniaxial specimens experimentally tested in the current investigation. The solid line in Fig. 11 was obtained by fitting the fully reversed uniaxial fatigue data using the three-parameter equation mathematically identical to Eq. (2). The dotted lines are the factor-of-five boundaries. It is clear that the parameter correlates the experiments well for most of the uniaxial loading cases. Exceptions are the those under the loading conditions with large compressive mean stresses. Several specimens were tested with a positive maximum stress being close to zero. As a result, the SWT fatigue parameter was very small according to Eq. (1). These are the data points shown in Fig. 11 that deviate significantly from the general tendency line. As has been well recognized, the SWT parameter assumes zero fatigue damage when the maximum stress is negative. The parameter fails to predict the fatigue failure under compression–compression that was experimentally observed. Since the logarithmic scale used, the specimens under compression-compression loading are not shown in Fig. 11.

Once the relationship between the FP and the fatigue life is established based on the fully reversed uniaxial loading, fatigue life can be predicted for any given loading condition

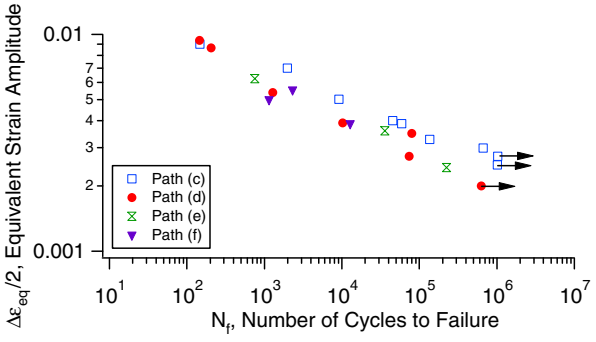

Fig. 10. Fatigue under combined axial-torsion loading.

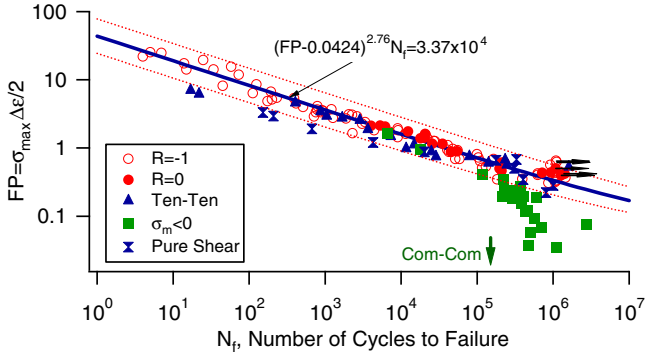

Fig. 11. SWT parameter versus fatigue life under uniaxial loading.

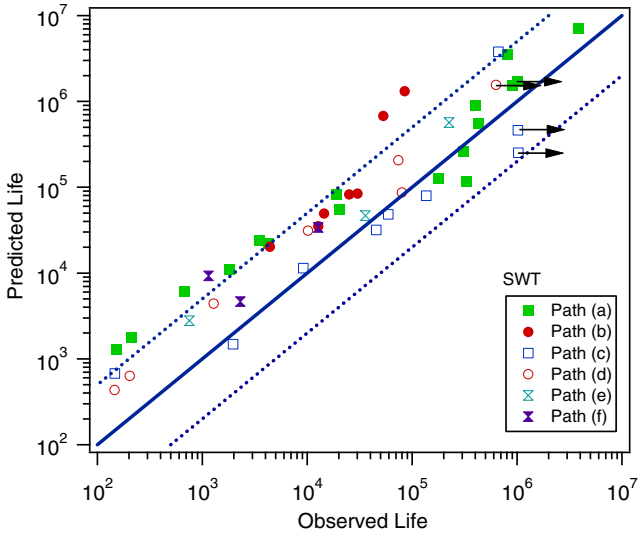

Fig. 12. SWT parameter correlation with experiments under combined axial-torsion loading.

when the stress and strain histories are known. Fig. 12 shows the comparison of the predicted fatigue life based on the SWT parameter and the observed life for all the tubular specimens tested in the current investigation. The stress and strain responses were obtained experimentally. Through a rotation of the coordinates system, the FP for any given material plane can be determined using the SWT parameter, Eq. (1). The maximum FP can be determined and the fatigue life can be obtained using the relationship between FP and the fatigue life (Fig. 11). At the same time, the orientation of the critical plane were determined.

The solid diagonal line in Fig. 12 denotes a perfect prediction. The two dotted lines are the factor-of-five boundaries. A glance at Fig. 12 reveals that the SWT parameter can correlate well the fatigue experiments under combined axial-torsion loading in terms of fatigue life. Among a total of 48 tubular specimens, the predicted fatigue lives of 38 specimens (79%) are within the factor-of-five lines, indicating a reasonable fatigue life prediction.

A critical plane approach is based upon the notion that a fatigue crack is initiated on a certain material plane where the fatigue damage is the maximum. Therefore, a critical plane approach can predict both the fatigue life and the critical planes where cracks are predicted to initiate. For an axial-torsion tubular specimen or a uniaxial tension–compression specimen, the material plane can be represented by its normal direction using one angle, θ, measured counter-clockwise from the axial direction (refer to the upper-right inset in Fig. 13). For a given loading condition, it is often found that several material planes or a range of material planes may experience identical or very similar fatigue damage according to a given fatigue criterion. Due to the inherent data scatter in fatigue experiments, it would be preferable to identify the material planes with similar fatigue damage by using a given fatigue criterion. In the current investigation, a range of 10% from the maximum fatigue damage is used for the discussion of possible cracking material planes predicted by a fatigue criterion. As shown in Fig. 13, the distribution of the fatigue damage per loading cycle over the material plane orientation can be determined according to a criterion for a given loading condition. The fatigue damage per loading cycle is the reciprocal of the predicted fatigue life under constant amplitude loading. The fatigue damage shown in Fig. 13 is normalized so that the maximum fatigue damage with respect to all the possible material planes is unit. Theoretically, the maximum peak points are predicted to be the critical planes and cracks are predicted to form on these particular material planes. By considering a range of 10% from the maximum fatigue damage, a range of the cracking directions can be obtained. It should be noted that a 10% range was arbitrarily selected without a physical consideration.

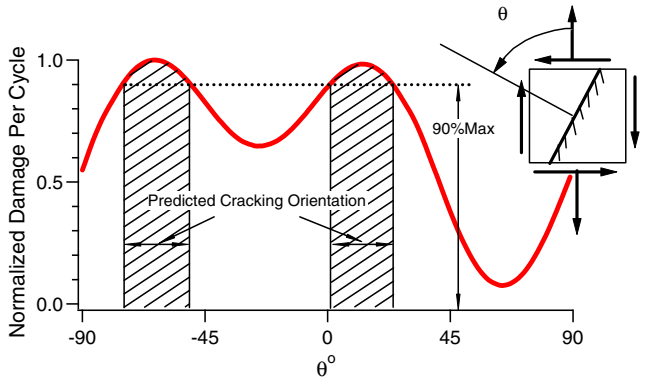

Fig. 13. Dependence of fatigue damage on material plane orientation.

Fig. 14 summarizes the comparison of the observed cracking directions and the predictions obtained from using the SWT fatigue criterion. The solid dots represent the observed crack orientations. The size of the dots signifies the general scatter existed in the experimental measurement of the cracking angle. The range bars in the figure are the predicted ranges of the cracking directions. Observations on the experimental cracking behavior were made in the millimeter scale of the crack length. As will be discussed in a later section, such a treatment is consistent with the macroscopic continuum assumption adopted in the current investigation for the stress and strain.

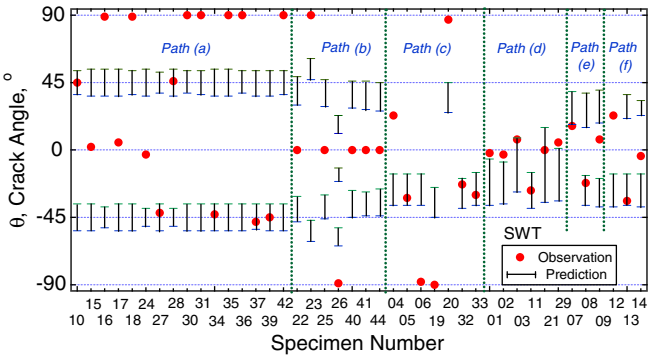

Fig. 14. Comparison of the experimentally observed cracking directions with the predictions by the SWT criterion.

The results in Fig. 14 show that among the 42 tubular specimens tested under axial-torsion loading, the SWT model can only predict correctly the cracking behavior for 15 specimens (36%). Such a poor predictability of the SWT criterion for cracking behavior is not surprising because the criterion predicts tensile cracking behavior while the material under investigation displays "diverse" cracking behavior. For the material subjected to uniaxial loading, the SWT criterion predicts a cracking plane that is perpendicular to the loading axis in the uniaxial specimen. For a specimen under cyclic torsion, the parameter predicts a crack plane with its normal making ±45° angle from the loading specimen axis. As shown in Figs. 5 and 9, 7075-T651 alloy displays different cracking behavior dependent on the loading magnitude or fatigue life. The SWT criterion can predict cracking direction correctly for both uniaxial and pure shear when the fatigue lives are longer than approximately 3×10^5 cycles.

4. Modified SWT parameter

Jiang and Sehitoglu [19] extended the SWT parameter to consider the general stress state and cracking behavior. With a slightly different form, the modified SWT criterion can be expressed by

$$FP = 2b\Delta\varepsilon\langle\sigma_{\max}\rangle + \frac{1-b}{2}\Delta\tau\Delta\gamma \tag{4}$$

where σ and τ are the normal stress and shear stress, respectively, on a material plane. ε and γ are the normal strain and shear strain corresponding to the normal stress, σ, and shear stress, τ, respectively. The symbol Δ denotes range in a loading cycle and the subscript "max" represents maximum in a loading cycle. Again, FP denotes "fatigue parameter." The symbol $\langle\rangle$ in Eq. (4) represents the MacCauley bracket (i.e., $\langle x\rangle = 0.5(x+|x|)$). The use of the MacCauley bracket is to ensure that no negative fatigue damage can be produced. The symbol b in Eq. (4) is a material constant and it ranges from 0 to 1.0. The critical plane is defined as the material plane which experiences the maximum fatigue damage. Accordingly, the critical plane is the material plane which has a maximum FP. Chu et al. [24] and Chu [25] developed a fatigue criterion mathematically identical to that of Eq. (4). A similar parameter was discussed by Glinka et al. [26].

For fully reversed uniaxial loading, the following equation can be derived with a coordinates rotation

$$\mathrm{FP} = \frac{1}{4}[b|1-\xi+(1+\xi)\cos 2\theta|(1+\cos 2\theta) + (1-b)(1+\xi)\sin^2 2\theta]\Delta\sigma_x\Delta\varepsilon_x \tag{5}$$

where θ is the angle made by the normal of the material plane and the axial stress direction (refer to the upper-right insert in Fig. 13). $\Delta\sigma_x$ is the axial stress range and $\Delta\varepsilon_x$ is the axial strain range in a loading cycle. The symbol ξ is the contraction ratio of the material under uniaxial loading. This contraction ratio can be obtained by using the following equation

$$\xi = \frac{\Delta\varepsilon_y}{\Delta\varepsilon_x} = 0.5\left(1-\frac{\Delta\sigma_x}{E\Delta\varepsilon_x}\right) + \mu\frac{\Delta\sigma_x}{E\Delta\varepsilon x} \tag{6}$$

where μ is the Poisson's ratio of the material. In deriving Eq. (6), the plastic incompressibility condition of the material has been used.

For fully reversed pure shear loading, the following relationship can be derived,

$$\mathrm{FP} = \frac{1}{2}[b\sin^2 2\theta + (1-b)\cos^2 2\theta]\Delta\tau_{xy}\Delta\gamma_{xy} \tag{7}$$

where $\Delta\tau_{xy}$ is the shear stress range and $\Delta\gamma_{xy}$ is the shear strain range in a loading cycle. θ denotes the angle made by the normal of the material plane and the axial direction. The graphic illustrations of Eqs. (5) and (7) are shown in Figs. 15 and 16 for fully reversed uniaxial loading and fully reversed pure shear loading, respectively. In these two figures, FP is normalized by $\Delta\sigma_x\Delta\varepsilon$ and $\Delta\tau_{xy}\Delta\gamma_{xy}$, respectively.

Clearly, the maximum FP and the critical plane orientation are dependent on the material constant, b. With Eqs. (5) and (7), the critical plane orientation can be determined by taking the derivative of with respect to the angle θ and letting the derivative be zero. To have a clear picture, Fig. 17 shows the dependence of the maximum FP on b for fully reversed tension–compression and pure shear. Fig. 17 suggests that the maximum FP under uniaxial loading decreases slightly and then increases with increasing b. For pure shear loading, the maximum FP decreases linearly with increasing

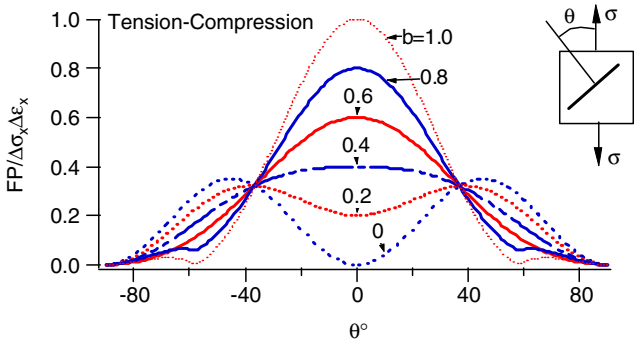

Fig. 15. Relationship between FP and the material plane orientation with different b values for fully reversed uniaxial loading.

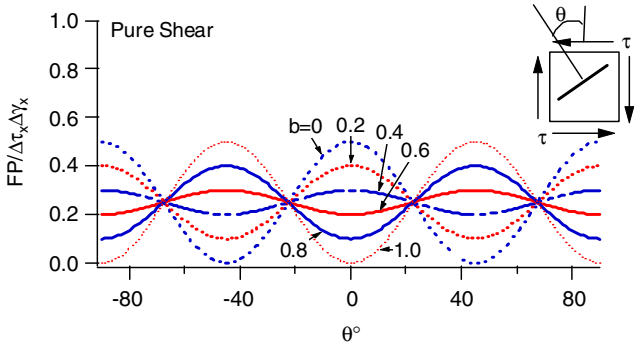

Fig. 16. Relationship between FP and the material plane orientation with different b values for fully reversed shear.

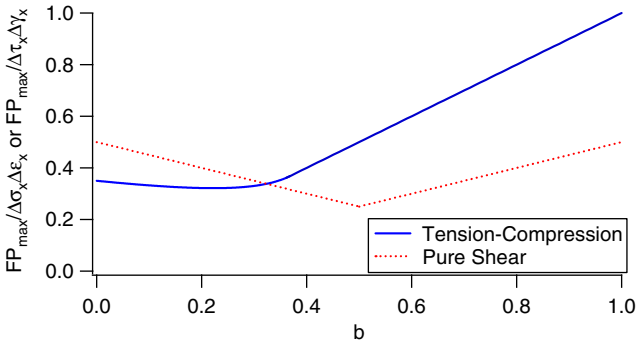

Fig. 17. Maximum FP as a function of b under fully reversed uniaxial and shear loading.

b when $b < 0.5$, and increases linearly with increasing b when $b > 0.5$. This ratio of the maximum FP under fully reversed uniaxial loading and that under fully reversed pure shear can help determine the material constant b.

Fig. 18 shows the orientation of the critical plane under the two typical loading conditions and the dependence of the critical plane on the material constant b. Experiments confirm that cracking behavior is material and loading magnitude dependent. To facilitate discussions, cracking behavior of a material can be classified into three types according to the cracking directions of the material under fully reversed tension–compression and pure shear loading. If fatigue cracks are initiated on the plane of maximum normal stress/strain range under both fully reversed uniaxial tension–compression and pure torsion, the cracking behavior is classified as "tensile cracking." If fatigue cracks are found on the material plane of maximum shear stress range for the pure shear loading and a material plane with its normal being oriented between zero and ±45° from the loading axis under uniaxial loading, the material is called to display shear cracking behavior. A material displays mixed cracking behavior if cracks are initiated on the maximum normal planes for tension–compression loading but on the maximum shear plane for torsion loading.

According the classification, it can be found in Fig. 18 that the modified SWT criterion can deal with materials displaying different cracking behavior. When $0.37 \geqslant b \geqslant 0$,

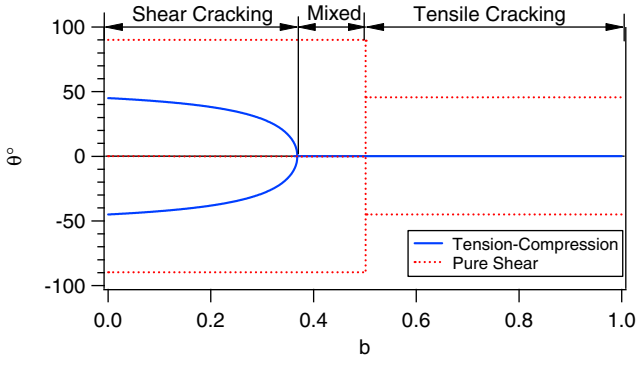

Fig. 18. Dependence of critical plane orientation on b for fully reversed uniaxial and pure torsion loading.

the criterion predicts shear cracking behavior. When $b \geqslant 0.5$, tensile cracking behavior is predicted. Mixed cracking behavior can be accounted for with a b value between 0.37 and 0.5. It is evident from Figs. 5 and 9 that the 7075-T651 aluminum alloy displays all the three different cracking types dependent on the fatigue life or loading magnitude. It should be noted that the classification of the cracking behavior into three types is based on the cracking behavior of a material under tension–compression and pure shear loading. It is difficult to label a material with a particular cracking behavior from the observation of the cracking behavior under more complicated loading condition, particularly considering the dependence of the cracking behavior on the loading magnitude.

4.1. Application of the modified SWT fatigue criterion to 7075-T651 aluminum alloy

The material constant b in the fatigue criterion, Eq. (4), is determined by comparing the fatigue results under fully uniaxial loading and those under fully reversed pure torsion fatigue of tubular specimens. Theoretically speaking, the FP-N_f (the number of loading cycles to failure) curves should coincide for a right choice of the material constant b. In addition, the selection of b should reflect the observed cracking behavior from the uniaxial loading and torsion loading.

Clearly, 7075-T651 displays cracking behavior that is dependent on the loading magnitude. Since the material constant b in the criterion describe the cracking behavior, a convenient and practical way is to relate the material constant b to the equivalent stress magnitude using a linear relationship

$$b = \langle a_1 - a_2\sigma_{eq} \rangle \tag{8}$$

where a_1 and a_2 are two constants that can be determined by the observed cracking behavior. The use of the MacCauley bracket is to ensure a non-negative b value. In addition, b should not be larger than unity.

σ_{eq} in Eq. (8) is the equivalent stress magnitude following the definition by Jiang and Kurath [29]. The mathematic expression for the equivalent stress magnitude is

$$\sigma_{eq} = \mathrm{Min}\left\{ \mathrm{Max}\sqrt{\frac{3}{2}(S_{ij} - S^0_{ij})(S_{ij} - S^0_{ij})} \right\} \tag{9}$$

where S_{ij} denotes the components of the deviatoric stress tensor and S^0_{ij} represents a point in the deviatoric stress space. The maximum inside the braces is taken with respect to the time within a loading cycle. The minimum is taken in terms of any possible point S^0_{ij} in the deviatoric stress space. Under tension–compression, the equivalent stress magnitude is equal to the stress amplitude. For pure shear loading, the equivalent stress magnitude is equal to the shear stress amplitude multiplied by $\sqrt{3}$.

Two points can be approximately identified from the cracking behavior observed on the material under fully reversed tension–compression and pure torsion. When the

fatigue life is 2000 cycles under fully reversed tension–compression loading, the material transits from shear cracking to mixed cracking (Fig. 5). The corresponding equivalent stress is 393 MPa. At this point, b should be equal to 0.37 according to aforementioned discussion on b [19]. From the pure torsion experiments, it can be identified that the material switches from mixed cracking to shear cracking when the fatigue life is in the region of 3×10^5 cycles (Fig. 9). Since the corresponding equivalent stress magnitude is 290 MPa, it can be identified that $b=0.5$ when $\sigma_{eq}=290$ MPa. With these two particular points for Eq. (8), $a_1=0.862$ and $a_2=0.00125$ were obtained for 7075-T651 aluminum alloy. Eq. (8) with the consideration of the dependence of the cracking behavior on the loading magnitude warrants that the modified SWT criterion will predict cracking behavior correctly for most of the uniaxial and shear specimens.

Fig. 19 shows the FP_{max}–N_f relationship for uniaxial loading and pure torsion. FP_{max} is the maximum FP value of Eq. (4) with respect to any possible orientations of the material plane. Again, a three-parameter relationship between FP_{max} and N_f mathematically identical to Eq. (2) is used to best fit the results experimentally obtained under fully reversed tension–compression. As shown in Fig. 19, this relationship serves as the baseline for comparison. The dotted lines are factor-of-five boundaries away from the baseline. Clearly, most of the experimental data points are within the factor-of-five boundaries. It should be noted that all the uniaxial experiments including those with high compressive mean stresses and compression-compression loading conditions have been included in Fig. 19.

Once the material constant b is selected, the critical plane and FP_{max} for each specimen conducted can be determined. Fig. 20 shows the comparison of the predicted fatigue lives and the experimentally observed fatigue lives of the tubular specimens subjected to axial-torsion loading. The stress and strain were obtained experimentally for each specimen. The solid line in Fig. 20 signifies a perfect prediction and the two dotted lines are the factor-of-five boundaries. Among the 48 tubular specimens tested with different axial-torsion loading paths, only one specimen is out of the factor-of-five lines.

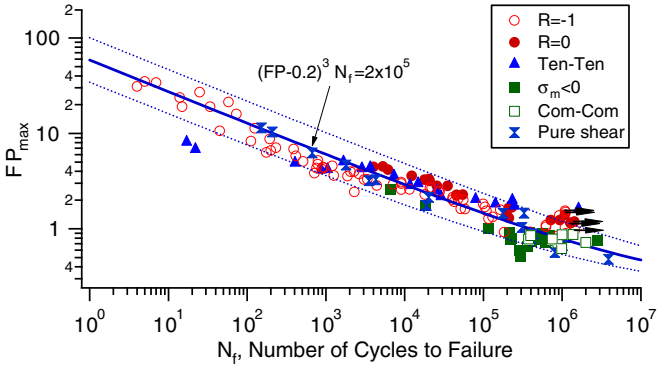

Fig. 19. FP_{max} versus N_f for uniaxial and torsion loading.

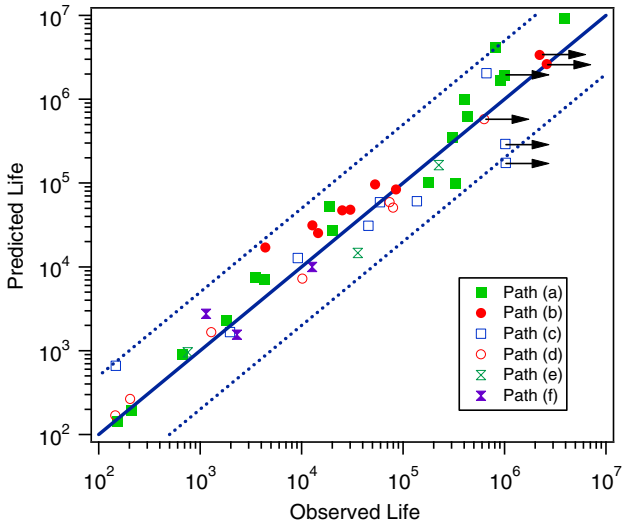

Fig. 20. Experimental observations versus predicted life obtained by using the criterion Eq. (4).

Fig. 21 summarizes the comparison of the observed cracking behavior and the predicted cracking orientations by the modified SWT fatigue criterion. The solid dark dots represent the observed crack orientations in the figure. The range bars in the figure are the predicted ranges of the cracking directions. Again, observations on the experimental cracking behavior were made in the millimeter scale of the crack length. The results shown in Fig. 21 reveal that the modified SWT criterion provides cracking direction predictions more satisfactorily than does the SWT criterion. Most of the cracking directions are predicted correctly. Among 42 tubular specimens presented in Fig. 21, the cracking directions of 35 specimens (83.3%) were predicted correctly.

It is noted that multiple critical planes can be predicted when using a critical plane approach. Fig. 22 shows the predicted FP versus the material plane orientation for specimen Tu08. The specimen was subjected to nonproportional loading with a loading path shown in Fig. 4e. The experiment was conducted under the stress-controlled loading condition. The axial stress amplitude was 147.5 MPa and the shear stress amplitude was 86.9 MPa. The observed fatigue life of this specimen was 225,000 cycles. Two peak

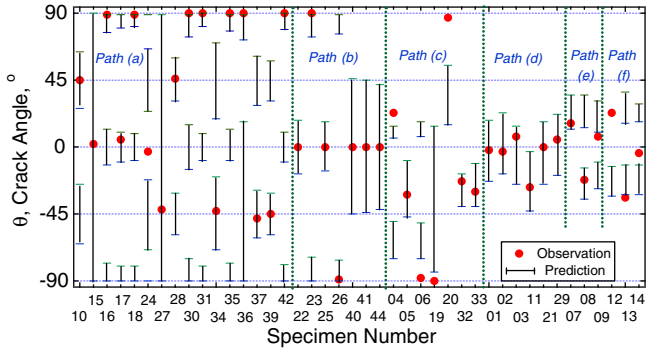

Fig. 21. Comparison of the experimentally observed cracking directions with the predictions made by using the modified SWT criterion.

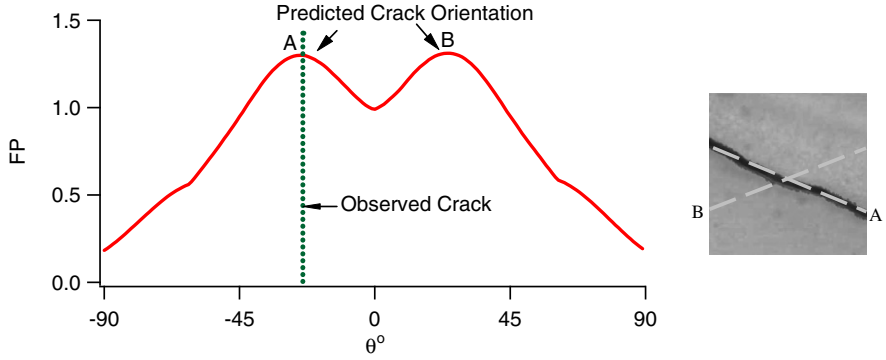

Fig. 22. Predicted *FP* as a function of the material plane orientation (Specimen Tu08).

values can be identified at "A" and "B," respectively, in Fig. 22. As a result, two critical planes are predicted. As shown on the right side picture in Fig. 22, the observed cracking orientation is consistent with the critical plane indicated by point "A."

It is possible that a great range of material planes can experience similar fatigue damage. Specimens Tu15 and Tu27 are two special cases where any material planes with their normal perpendicular to the radial direction of the tubular specimen are predicted to experience very similar fatigue damage. As a result, the predicted crack can be on any of these material planes. This is because for these two pure torsion specimens the stress amplitudes are at the level which results in the material constant b being approximately 0.5. It is noted from Eq. (7) that the fatigue damage is independent of the angle θ when $b = 0.5$.

5. Discussion

The experiments conducted in the current investigation confirm that significant fatigue damage can be produced under compression–compression loading for the 7075-T651 aluminum alloy. Usually, a material is dominated by one type of cracking behavior. In contrast, 7075-T651 aluminum alloy displays shear cracking, mixed cracking, and tensile cracking dependent on the loading magnitude. Earlier investigations indicate that many materials are dominated by mixed cracking behavior [19,27,28], and few, such as stainless steels, exhibit primarily tensile cracking behavior [20]. Very few materials display predominant shear cracking behavior [30]. One characteristic of the fatigue behavior of 7075-T651 is the distinct kink observed in the shear strain versus fatigue life curve (Fig. 9) that is accompanied by the change of cracking behavior. To the best of the authors' knowledge, such a torsion fatigue behavior has never been documented for an aluminum alloy when the fatigue life is less than 10^7 cycles, although it would not be a surprise according to Socie [31]. A kink was observed in the strain–life curve of an induction hardened steel where the gradient material properties resulted in subsurface cracking [32].

When discussing the fatigue initiation cracking direction, there exist different opinions with regard to the definition of the experimentally observed cracking direction due to the inherent roughness of the crack surface. The current investigation adopts a macroscopic crack definition with the crack length being in the millimeter scale. This is because the stress and strain used in most fatigue criteria are based upon the traditional continuum mechanics concepts. A polycrystalline material consists of grains that are oriented in different directions. An implicit assumption in macroscopic continuum mechanics is that a material point is small enough so that it can be treated as a mathematical point but it is large enough to contain at least several grains so that the material can be treated as homogeneous. In other words, the stress and strain are defined in a macroscopic level. Considering the general range of the grain size of a metallic polycrystalline material, the size of the basic material "element" should be in the millimeter scale rather than the micrometer scale. As a result, discussions on cracking behavior in the current article are limited to the visible and macroscopic cracks.

Many fatigue criteria have been proposed. A development in the last few decades is the confirmation of the critical plane approaches. The general concept of a critical plane approach is the consistency of the fatigue damage with the observed dependence of the cracking behavior on the stress state and the loading path. Accordingly, a critical plane approach can not only predict fatigue life but also the material plane where the fatigue crack is initiated. Generally, the critical plane approaches were developed for materials displaying either shear cracking or tensile cracking. For example, the Fatemi–Socie criterion [33] is for shear cracking materials and the SWT criterion with the critical plane interpretation by Socie [15] is suitable for materials displaying tensile cracking.

It has been widely accepted that the SWT criterion particularly works well for the aluminum alloys. The current investigation suggests that the SWT criterion can predict fatigue life reasonably well for most of the fatigue experiments conducted in the current study. It confirms an early conclusion that the criterion cannot correctly predict the tension–compression cases with the maximum stress being very low. It is obvious that the criterion does not predict fatigue failure under compression–compression loading. More importantly, the criterion fails to predict correct cracking directions of most specimens investigated.

The modified SWT criterion, Eq. (4), integrates both the normal components and the shear components of the stress and strain on a material plane. The two terms are combined using a material constant b which ranges from 0.0 to 1.0. When b equals 1, the criterion is identical to the SWT criterion. When $b = 0$, the criterion is for a material that the normal stress and strain components do not contribute to fatigue damage on a material plane. Since the criterion is an extension of the SWT fatigue parameter, the good consideration of the mean stress effect is inherited. One of the advantages of using the SWT criterion is that the baseline can be fully determined from the fully reversed tension–compression fatigue experiments. This is because the SWT criterion contains no material constants. Clearly, the introduction of the material constant, b, in Eq. (4), will require more fatigue experiments in order to determine it. However, this material constant is necessary to consider the varying cracking behavior of the material with the loading magnitude.

A significant improvement is achieved with the modified SWT criterion in terms of life prediction and cracking direction prediction. The results shown in Fig. 19 indicate that the modified SWT criterion can consider the mean stress effect fairly well for all the experiments conducted in the current study. Since the selection of the material constants a_1 and a_2 in Eq. (8) has incorporated the dependence of the observed cracking behavior on the loading magnitude, the modified SWT criterion correlates well the fully reversed tension–compression and pure shear experiments in terms of the cracking directions. For the tubular specimens subjected to combined axial-torsion loading, the predictions of the fatigue life and cracking direction have been also improved when comparing Fig. 20 with Figs. 12 and 21 with Fig. 14.

Although the modified SWT criterion can predict fatigue failure under the compression–compression loading, it should be noted that the criterion is not able to properly predict the cracking direction under compression–compression. The cracking surface in the compression–compression specimen was found to be perpendicular to the loading axis while the predicted cracking surface has its normal being $\pm 45^\circ$ to the loading axis.

Jiang [27] developed a critical plane multiaxial fatigue criterion that incorporates both the shear and normal stress and strain components on a material plane. The criterion is based upon the plastic deformation and is in an incremental form. Comparing the modified SWT criterion, Eq. (4), with the multiaxial fatigue criterion developed by Jiang [27], it can be found that both models consider mean stress effect and can be used for materials displaying different cracking behavior. An obvious advantage of the incremental fatigue criterion by Jiang [27] is the elimination of a cycle-counting method for any general loading histories. On the other hand, cyclic plasticity is necessary for fatigue to occur in the incremental fatigue criterion. Therefore, the incremental fatigue criterion is difficult to use for a material that displays very small or minimal cyclic plasticity in the high cycle fatigue regime. An advantage of the fatigue parameter of Eq. (4) can be applied for a material that does not have significant cyclic plasticity. However, the SWT criterion and its modification use stress/strain quantities such as strain amplitude and maximum stress that are based on the definition of a loading cycle or reversal. As a result, a cycle-counting method is needed to assess fatigue damage under variable amplitude loading conditions. Currently, the only accepted cycle-counting method that is designed to find the closed stress–strain hysteresis loops in a loading history. For uniaxial loading, the use of the rain-flow method to identify a cycle or reversal is straightforward. However, when the rain-flow counting method is used for nonproportional multiaxial loading, difficulties arise because the stress and strain quantities on a material plane may not form consistent stress–strain hysteresis loops for normal and shear components. On a given material plane or direction, both the magnitude and direction of the shear components may vary with time.

A successful critical plane approach should be able to predict both the fatigue life and the dominant failure planes. An earlier investigation of three different critical plane approaches reveals that the cracking direction is more difficult to predict than the fatigue life [34]. The current investigation affirms such a conclusion. The SWT criterion can predict fatigue lives reasonably well but it does not predict correct cracking directions for most of the specimens investigated in the current study. The modified SWT criterion improves the predictions in both fatigue life and cracking direction. It can predict the fatigue lives of most of the specimens within the factor-of-five range, noting that such a range is similar to the scatter of the experimental fatigue data obtained for tension–compression (Fig. 5). The prediction of the cracking behavior of the material by the modified criterion is not as desirable.

While uniaxial and pure shear fatigue experiments are often used to provide the baseline fatigue data for a material, the two basic loading modes also provide the basic cracking behavior. The cracking behavior of a material can be classified according to the observations of the specimens under fully reversed tension–compression and pure shear loading. The transition of cracking behavior from one type to another due to the change of loading magnitude has been well recognized. However, the cracking behavior under the two basic loading modes has not been well considered in the development of the critical plane multiaxial fatigue models. In fact, the cracking behavior observed on the two basic loading modes can serve as the critical observations to evaluate a critical plane approach. If a critical plane approach is not able to mimic the cracking behavior observed under fully reversed tension–compression and pure shear, its capability to predict cracking behavior under more general stress states is naturally in doubt. The rich cracking behavior observed on the aluminum alloy can serve as benchmark experiments that can be used to critically evaluate a critical plane approach.

6. Conclusions

A systematic experimental investigation was conducted on the fatigue behavior of 7075-T651 aluminum alloy under the uniaxial, torsion, and axial-torsion loading conditions. The mean stress has a significant effect on fatigue life. Fatigue damage was found to occur under compression-compression loading. The material displays shear cracking, mixed cracking, and tensile crack behavior dependent on the loading magnitude. The Smith, Watson, and Topper (SWT) fatigue criterion can predict the fatigue life well for most of the experiments except those with very low or negative maximum stresses. However, the SWT parameter does not predict correctly the cracking behavior for most of the specimens. A modified SWT criterion combines the normal and shear components of the stresses and strains on material planes. The modified criterion significantly improves the predictions of the fatigue life and cracking behavior.

Acknowledgements

The Missile Defense Agency (F49620-03-1-342) and the Office of Naval Research (N000140510777) sponsor this work. The views and conclusions contained herein are those of the authors and should not be interpreted as necessarily representing the official policies or endorsements, either expressed or implied, of the Missile Defense Agency, the Air Force Office of Scientific Research, the Office of Naval Research, or the US government.

References

[1] Hoffman ME, Hoffman PC. Current and future fatigue life prediction methods for aircraft structures. Navel Res Rev 1998;50(4):55–68.
[2] Jiang Y, Feng M. Modeling of fatigue crack propagation. ASME J Engng Mater Tech 2004;126:77–86.
[3] Endo T, Morrow J. Cyclic stress–strain and fatigue behavior of representative aircraft metals. J Mater JMLSA 1969;4(1):159–75.
[4] Boller CHR, Seeger T, editors. Materials data for cyclic loading, Part D: aluminum and titanium alloys. NY: Elsevier; 1987. p. 69–77.
[5] Boller CHR, Seeger T, editors. Materials data for cyclic loading, Part D: aluminum and titanium alloys. NY: Elsevier; 1987. p. 81–9.
[6] Bergmann JW. Zur Betriebsfestigkeitsbemessung gekerbter Bauteile auf der Grundlage der ortlichen Beanspruchungen. Veroffentilichungen des Instituts fur stahlbau und Werkstoffmechanik d. TU Darmstadt, 1983; Heft 37.
[7] Sanders Jr TH, Mauney DA, Staley JT. In: Jaffee RI, Wilcox BA, editors. Strain control fatigue as a tool to interpret fatigue initiation of aluminum alloys. Fundamental aspects of structural alloy design. NY (USA): Plenum; 1977.
[8] Fatemi A, Plaseied A, Khosrovaneb AK, Tanner D. Application of bi-linear log–log S–N model to strain-controlled fatigue data of aluminum alloys and its effect on life predictions. Int J Fatigue 2005;27:1040–50.
[9] Newman JC. A review of modeling small crack behavior and fatigue-life prediction for aluminum alloys. Fat Fract Engng Mater Struct 1994;17(4):429–39.
[10] Gill SJ, Pao PS. A method for conducting automated fatigue crack initiation tests on fracture mechanics specimens. In: Braun AA, Mckeighan PC, Nicolson AM, Lohr RD, editors. Applications of automation technology in fatigue and fracture testing and analysis. ASTM STP 1411, vol. 4. West Conshohocken (PA): American Society for Testing and Materials; 2002.
[11] Döring R, Hoffmeyer J, Seeger T, Vormwald M. Short fatigue crack growth under nonproportional multiaxial elastic–plastic strains. Int J Fatigue 2006;28:972–82.
[12] DeBartolo EA, Hillberry BM. A model of initial flaw sizes in aluminum alloys. Int J Fatigue 2001;23:S79–86.
[13] Xue Y, Jordon B, Horstemeyer S, Horstemeyer MF. Fatigue experiments, damage evaluation and multiscale modeling for AA 7075-T651. In: Proceedings of the 2005 SEM annual conference and exposition on experimental and applied mechanics, 2005; p. 1443–50.
[14] Smith RN, Watson P, Topper TH. A stress–strain parameter for the fatigue of metals. J Mat 1970;5(4):767–78.
[15] Socie DF. Multiaxial fatigue damage models. ASME J Engng Mater Tech 1987;109:293–8.
[16] Nadai A. Theory of low and fracture of solids, second ed., vol. 1. New York, Toronto, and London: McGraw-Hill Book Company, Inc.; 1950.
[17] Sakai Tatsuo, Sakai Takashi, Okada K, Furuichi M, Nishikawa I, Sugeta A. Statistical fatigue properties of SCM435 steel in ultra-long-life regime based on JSMS database on fatigue strength of metallic materials. Int J Fatigue 2006;28:1486–92.
[18] Marines I, Bin X, Bathias C. A understanding of very high cycle fatigue of metals. Int J Fatigue 2003;25:1101–7.
[19] Jiang Y, Sehitoglu H. Fatigue and stress analysis of rolling contact. Report no. 161, UILU-ENG 92-3602, College of Engineering, University of Illinois at Urbana-Champaign, 1992.
[20] Socie DF. Critical plane approaches for multiaxial fatigue damage assessment. In: McDowell DL, Ellis R, editors. Advances in multiaxial fatigue. ASTM STP vol. 1191, 1993; p. 7–36.
[21] Socie DF, Kurath P, Koch J. A multiaxial fatigue damage parameter. In: Miller KJ, Brown MW, editors. Biaxial and multiaxial fatigue. EGF3. London: Mechanical Engineering Publications; 1989. p. 535–50.
[22] Hua CT, Socie DF. Fatigue damage in 1045 steel under variable amplitude biaxial loading. Fatigue Eng Mater Struct 1985;8(2):101–4.
[23] Segan E. Corrosion fatigue of 7005-T53 aluminium alloy. PhD. Thesis, 1989.
[24] Chu CC, Conle FA, Bonnen JJ. Multiaxial stress–strain modeling and fatigue life prediction of SAE axle shafts. In: McDowell DL, Ellis R, editors. Advances in multiaxial fatigue. ASTM STP vol. 1191. Philadelphia: American Society for Testing and Materials; 1993. p. 7–54.
[25] Chu CC. Fatigue damage calculation using the critical plane approach. ASME, J Eng Mat Tech 1993;117:41–9.
[26] Glinka G, Shen G, Plumtree A. A multi-axial fatigue strain energy density parameter related to the critical fracture plane. Fatigue Fract Eng Mat Struct 1995;18:37–46.
[27] Jiang Y. A fatigue criterion for general multiaxial loading. Fat Fract Engng Mater Struct 2000;23:19–32.
[28] Zhang J, Jiang Y. Fatigue of polycrystalline copper with different grain sizes and texture. Int J Plast 2006;22:536–56.
[29] Jiang Y, Kurath P. Non-proportional cyclic deformation: critical experiments and analytical modeling. Int J Plast 1997;13:743–63.
[30] Socie DF, Waill LA, Dittmer DF. Biaxial fatigue of Inconel 718 including mean stress effects. In: Miller KJ, Brown MW, editors. Multiaxial fatigue, ASTM STP vol. 853, 1985; p. 463–81.
[31] Socie, DF. Private Communication; 2006.
[32] Kurath P, Jiang Y. Analysis of residual stresses and cyclic deformation for induction hardened components. Recent developments in fatigue technology. In: Chernenkoff RA, Bonnen JJ, editors. SAE, Warrendale, (PA); 1997, p. 337–51.
[33] Fatemi A, Socie DF. A critical plane approach to multiaxial fatigue damage including out of phase loading. Fat Fract Engng Mater Struct 1988;11:149–65.
[34] Jiang Y, Hertel O, Vormwald M. An experimental evaluation of three critical plane multiaxial fatigue criteria. Int J Fatigue 2007;29(8):1490–502.